

Regulation of mitochondrial fission by GIPC-mediated Drp1 retrograde transport

Aaron Ramonett^a, Eun-A Kwak^a, Tasmia Ahmed^b, Paola Cruz Flores^b, Hannah R. Ortiz^a, Yeon Sun Lee^a, Todd W. Vanderah^a, Tally Largent-Milnes^a, David F. Kashatus^c, Paul R. Langlais^d, Karthikeyan Mythreye^e, and Nam Y. Lee^{a,b,f,*}

^aDepartment of Pharmacology, ^bDepartment of Chemistry & Biochemistry, ^dDepartment of Medicine, and ^fCancer Center, University of Arizona, Tucson, AZ 85724; ^cDepartment of Microbiology, Immunology and Cancer Biology, University of Virginia, Charlottesville, VA 22908; ^eDepartment of Pathology, University of Alabama at Birmingham, 35294

ABSTRACT Dynamin-related protein 1 (Drp1) is a key regulator of mitochondrial fission, a large cytoplasmic GTPase recruited to the mitochondrial surface via transmembrane adaptors to initiate scission. While Brownian motion likely accounts for the local interactions between Drp1 and the mitochondrial adaptors, how this essential enzyme is targeted from more distal regions like the cell periphery remains unknown. Based on proteomic interactome screening and cell-based studies, we report that GAIP/RGS19-interacting protein (GIPC) mediates the actin-based retrograde transport of Drp1 toward the perinuclear mitochondria to enhance fission. Drp1 interacts with GIPC through its atypical C-terminal PDZ-binding motif. Loss of this interaction abrogates Drp1 retrograde transport resulting in cytoplasmic mislocalization and reduced fission despite retaining normal intrinsic GTPase activity. Functionally, we demonstrate that GIPC potentiates the Drp1-driven proliferative and migratory capacity in cancer cells. Together, these findings establish a direct molecular link between altered GIPC expression and Drp1 function in cancer progression and metabolic disorders.

Monitoring Editor

Anne Spang
University of Basel

Received: Jun 3, 2021

Revised: Oct 19, 2021

Accepted: Oct 21, 2021

INTRODUCTION

Mitochondrial morphology and distribution are key determinants of metabolism governed by the continuous interplay of fusion and fission (Archer, 2013; Ranieri *et al.*, 2013; Lackner, 2014). Fusion requires three large GTPases of the dynamin superfamily, mitofusins 1 and 2 (Mfn1 and Mfn2) and optic atrophy 1 (Opa1), which mediate outer and inner mitochondrial membrane fusion, respectively (Hales and Fuller, 1997; Chen *et al.*, 2003; Cipolat *et al.*, 2004). Dynamin-related protein 1 (Drp1) is the central mediator of fission, a cytosolic GTPase that is recruited to the mitochondrial surface in response to metabolic changes, stress, and growth factor stimuli (Frank *et al.*, 2001). On translocation, Drp1 assembles into oligomeric complexes at sites precontracted by actin and nonmuscle myosin II to initiate membrane scission.

This article was published online ahead of print in MBoC in Press (<http://www.molbiolcell.org/cgi/doi/10.1091/mbc.E21-06-0286>) on October 27, 2021.

Competing interest statement: Authors declare no competing interests.

Author contributions: A.R. conducted the majority of the experiments and data analysis as first author; E.K., T.A., and P.C.F. performed biochemical experiments and generated stable cell lines; P.R.L. provided MS proteomics data analysis; D.F.K. provided the Drp-null and control mouse PDAC cells; Y.S.L., T.W.V., T.M.L., and K.M. assisted with experimental procedures and edited the paper; N.Y.L. conceived the study and edited the paper with contributions from A.R.

Declaration of interests: The authors declare no conflict of interests.

*Address correspondence to: Nam Y. Lee (namlee@email.arizona.edu).

Abbreviations used: BSA, bovine serum albumin; Drp, dynamin-related protein; ER, endoplasmic reticulum; FBS, fetal bovine serum; GIPC1, GAIP/RGS19-interacting protein; MFF, mitochondrial fission factor; Mfn, mitofusin; MiD, mitochondrial dynamics protein; MYO6, myosin VI; Opa, optic atrophy; PBS, phosphate-buffered saline; PDAC, pancreatic ductal adenocarcinoma; PTM, posttranslational modification; ROI, region of interest; ROS, reactive oxygen species; TBS, Tris-buffered saline; WT, wild type.

© 2022 Ramonett *et al.* This article is distributed by The American Society for Cell Biology under license from the author(s). Two months after publication it is available to the public under an Attribution–Noncommercial–Share Alike 4.0 International Creative Commons License (<http://creativecommons.org/licenses/by-nc-sa/4.0>).

“ASCB®,” “The American Society for Cell Biology®,” and “Molecular Biology of the Cell®” are registered trademarks of The American Society for Cell Biology.

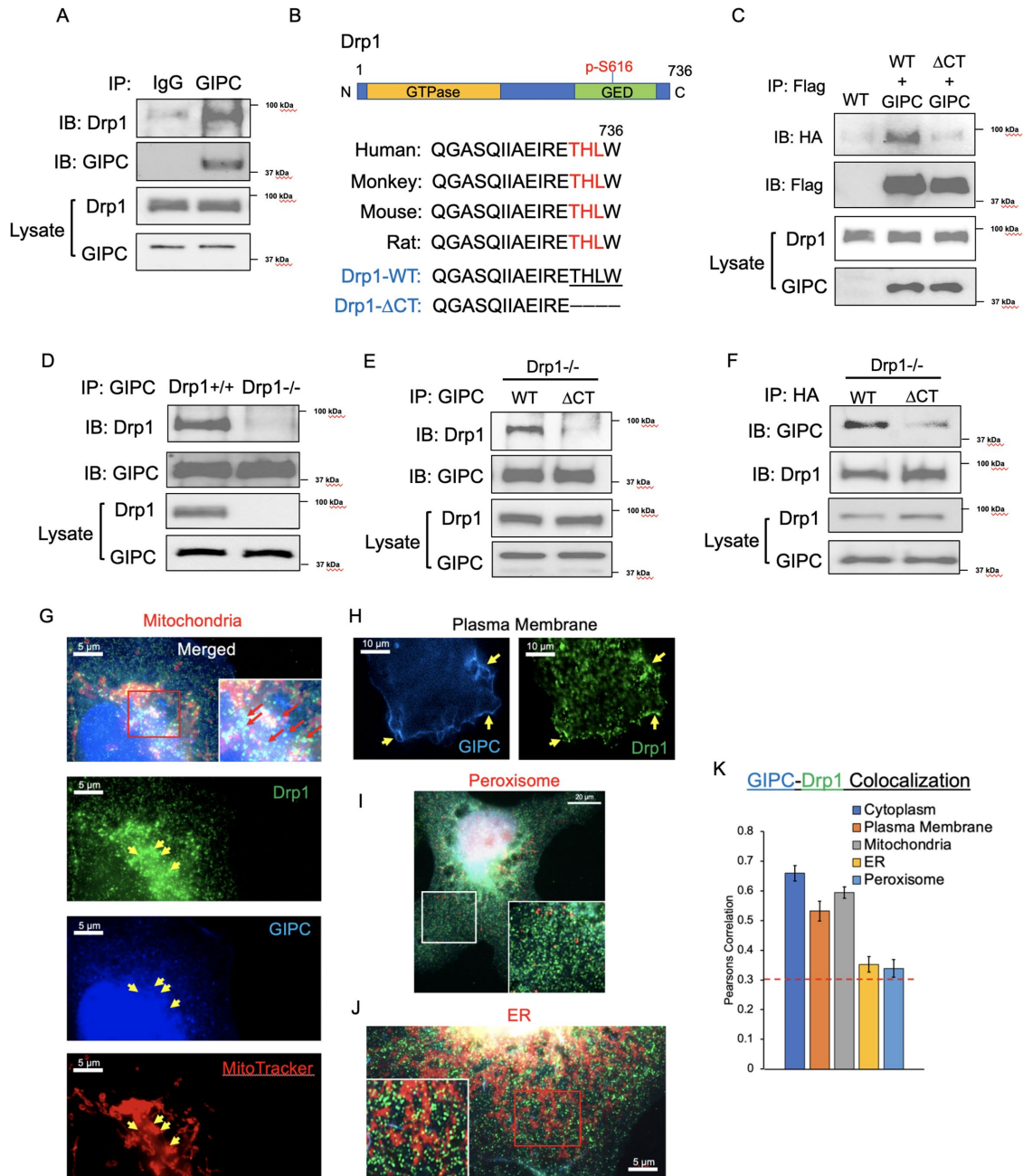


FIGURE 1: Drp1 interacts with GIPC via C-terminal PDZ-binding motif. (A) Immunoprecipitation of endogenous GIPC results in coprecipitation of endogenous Drp1 in COS7 cells. Immunoblots shown are representative of at least three independent experiments. (B) Schematic representation of Drp1 and its conserved C-terminal peptide residues across species. The last three of four amino acids (red) matches the conserved type I PDZ binding motif. Comparison of Drp1-WT vs. Drp1- Δ CT reveals the truncation sequence (dotted lines). (C) Immunoprecipitation of Flag-tagged GIPC shows coprecipitation of HA-tagged Drp1-WT but not HA-Drp1- Δ CT. Immunoblots are representative of at least four independent experiments. (D) Immunoprecipitation of endogenous GIPC results in coprecipitation of endogenous Drp1 in Drp1^{+/+} control primary mouse PDAC cells but not in Drp1-null (Drp1^{-/-}) PDAC cells. Immunoblots shown are representative of at least three independent experiments. (E) Rescue experiment wherein Drp1-null cells are transfected with Drp1-WT or Drp1- Δ CT. Immunoprecipitation of endogenous GIPC results in coprecipitation of Drp1-WT but not Drp1- Δ CT. Immunoblots shown are representative of at least four independent experiments. (F) Reciprocal rescue experiment shows immunoprecipitation of ectopically expressed Drp1-WT or Drp1- Δ CT in Drp1-null PDAC cells, resulting in endogenous GIPC coprecipitation in WT but not Δ CT. Immunoblots shown are representative of at least three independent experiments. (G) Immunofluorescence images show ectopic expression of Flag-GIPC (blue), endogenous Drp1 (green) and MitoTracker (red) in COS7 cells. Merged image and inset panels with red arrows indicate colocalization of all three in white clusters. (H) Immunofluorescence images of Flag-GIPC (blue) and Drp1 (green) in COS7 cells show their colocalization at the plasma membrane (yellow arrows). (I) COS7 cells overexpressing Flag-GIPC and peroxisome reporter mScarlet, were stained for Flag (blue) and Drp1 (green). Inset image shows little colocalization of GIPC and Drp1 near peroxisomes. (J) COS7 cells overexpressing Flag-GIPC and ER-RFP, were stained for Drp1

Chang and Blackstone, 2010; Breitzig *et al.*, 2018). Ser616 and Ser637 are arguably the two most extensively characterized sites, with Ser616 phosphorylation by cdk1, ERK, PKC, and CaMKII causing Drp1-induced mitochondrial fission, whereas PKA phosphorylation of Ser637 inhibits this process (Chang and Blackstone, 2007a, b; Santel and Frank, 2008; Kashatus *et al.*, 2015; Serasinghe *et al.*, 2015).

GIPC1 (GAIP/RGS19-interacting protein) is a highly versatile adaptor protein involved in trafficking, signaling and recycling of transmembrane receptors and cytosolic protein complexes (Ahmed *et al.*, 2021; Katoh, 2013). To date, over 50 protein interactions have been reported including GPCRs, IGF-1R, and endosomal scaffolding molecules such as APPL1, which binds to the central PDZ domain of GIPC through their extreme C-terminal PDZ ligand motif comprising the consensus (S/T)-X-(A/V) peptide sequence or variations thereof (Ahmed *et al.*, 2021). In addition, GIPC can interact with myosin VI (MYO6), the only member of the myosin superfamily that translocates to the minus-end of actin filaments (Wells *et al.*, 1999). This unique directionality provides retrograde trafficking of endocytic vesicles and protein cargo along actin filaments. As such, the GIPC1-MYO6 complex proves essential for regulating certain growth factor signaling, cell motility, and other vital functions during neuronal and cardiovascular development (Naccache *et al.*, 2006; Valdembrri *et al.*, 2009; Lee *et al.*, 2012; La Torre *et al.*, 2015).

In cancer, GIPC reportedly has prominent yet complex differential roles (Ahmed *et al.*, 2021). Although frequently overexpressed in breast, pancreatic, and ovarian tumors, among others, it can either promote or inhibit the overall tumorigenicity depending on cellular contexts and its preferential interactions with various receptors and signaling complexes that control cell growth, migration, and invasion (Chittenden *et al.*, 2010; Lee *et al.*, 2010). More recent studies have explored GIPC as a target including cell-permeable peptides that bind the PDZ domain to block protein–protein interactions (Muders *et al.*, 2009; Pal *et al.*, 2014). While most current anticancer agents function by directly binding to intracellular kinases or cell surface receptors, the disruption of such cytosolic PDZ-dependent protein interactions represents an emerging field for cancer therapeutics.

Despite recent advances, a fundamental question regarding Drp1 is how this cytosolic enzyme translocates to the mitochondrial surface, whether it relies primarily on Brownian motion for local targeting to nearby mitochondria where it can interact with the fission machinery, or whether it possesses more regulated directed movements for medium- or long-range transport from more distal sites like the cell periphery. Based on proteomic interactome and analysis of Drp1 subcellular distribution, we report that GIPC is required for the retrograde Drp1 trafficking toward the perinuclear mitochondria. We demonstrate the molecular basis for the transport process, its overall role in mitochondrial dynamics, and unique implications for cancer and many metabolic disorders.

RESULTS

As GIPC has the capacity to differentially interact with multiple binding partners, we aimed at profiling the strength and duration of their interactions in normal and cancer cell contexts via mass spectrometry quantitative interactome studies. Several potentially new pro-

tein interactions were identified including Drp1, which forms the basis of the present study. To confirm this interaction, coimmunoprecipitation was performed first in an endogenous setting where GIPC immunoprecipitation resulted in strong coprecipitation of Drp1 relative to IgG control (Figure 1A). Accordingly, we reasoned that Drp1 might be a PDZ-domain substrate since its extreme C-terminal residues are conserved across species and comprised THLW as the last four amino acid residues that partially matched the consensus PDZ-binding motif sequence ending with a hydrophobic residue (Figure 1B). To test whether the GIPC–Drp1 interaction is mediated by this putative motif, we truncated the last four THLW residues (Drp1- Δ CT) then overexpressed an HA-tagged form of this mutant to find its interaction abrogated relative to the HA-tagged wild-type (WT) control (Figure 1C).

To exclude the possibility of endogenously expressed Drp1 oligomerizing with the ectopically expressed Drp1- Δ CT, subsequent studies were conducted in Drp1-null cells. Here, primary tumor cells previously isolated from genetically engineered pancreatic ductal adenocarcinoma (PDAC) mice with Drp1 gene deletion were chosen as a model system (Nagdas *et al.*, 2019). We first confirmed the specificity of their endogenous interaction wherein GIPC robustly interacted with Drp1 in Drp1+/+ but not Drp1-null cells (Figure 1D). Rescue experiments where Drp1-null cells reconstituted with either WT or Drp1- Δ CT showed selective interaction with endogenous GIPC in the former but not the latter irrespective of whether immunoprecipitated for GIPC or Drp1, thus demonstrating that the GIPC–Drp1 interaction is mediated by the conserved C-terminal residues of Drp1 that acts as a PDZ-binding motif (Figure 1, E and F).

Aside from its prominent cytosolic and mitochondrial distributions, previous studies have shown that Drp1 can also localize at the plasma membrane, the endoplasmic reticulum (ER), and peroxisome (Ji *et al.*, 2017; Kraus and Ryan, 2017; Kamekar *et al.*, 2018). Having established the GIPC–Drp1 interaction biochemically, we next tested where the GIPC–Drp1 complex is primarily localized in intact cells through visualization of their colocalization within each of the aforementioned cellular compartments (Figure 1G). Here, ectopically expressed GIPC (blue) showed significant colocalization with endogenous Drp1 (green) at the mitochondria (red), which when merged together, yielded white fluorescence emission (Figure 1G, merged panel and inset panel showing white clusters with red arrows). Indeed, the Pearson correlation analysis of their tristaining yielded a value of nearly 0.7, a coefficient value that reflects robust colocalization compared with those typically below 0.3 that indicate random distribution (Figure 1K). Similarly, their strong colocalization was observed in the cytoplasm and along the plasma membrane but to a much lesser degree within the ER or peroxisome (Figure 1, H–K; Supplemental Figure S1B), suggesting that the GIPC–Drp1 interaction occurs mostly at the membrane and mitochondria in the cytoplasm.

Given the above findings, we tested whether GIPC influences Drp1 trafficking. Initial immunofluorescence studies in COS7 cells revealed a fairly diffuse cytoplasmic distribution of endogenous Drp1, whereas GIPC overexpression resulted in its striking redistribution into perinuclear clusters (Figure 2A, a and b, white arrows). Moreover, costaining with MitoTracker confirmed this clustering to represent Drp1 accumulation near the main mitochondrial body,

(green) and Flag (blue). Zoomed image shows little colocalization of GIPC and Drp1 near the ER. (K) The graph represents the unbiased Pearson correlation coefficient of GIPC and Drp1 colocalizing in different compartments. Coefficients were calculated for GIPC and Drp1 in the cytoplasm, plasma membrane, mitochondria, ER, and peroxisomes. Twenty-five cells were quantified per group with two to three ROIs per cell.

which was markedly fragmented and condensed around the perinucleus compared with untransfected control. In fact, by plotting the varying levels of GIPC expression quantified for each cell against form factor, a metric of mitochondrial fusion (Dagda *et al.*, 2009; Kumar *et al.*, 2016), an inverse correlation was noted wherein increasing GIPC levels resulted in a proportionate decrease in mitochondrial fusion, thus suggesting that GIPC promotes mitochondrial fission through its interaction with Drp1 (Figure 2B, downward slope line). To perform a reciprocal experiment in which endogenous GIPC is silenced, we chose MiaPaca2, a human PDAC cell line with characteristically high expression of both GIPC and Drp1 expression (Figure 2C). As reported previously in MiaPaca2 and most other PDAC cell types, Drp1 accumulated in the perinuclear regions accompanied by a considerable level of mitochondrial fission as revealed by MitoTracker (Figure 2C, green and red in top inset panels) (Nagdas *et al.*, 2019; Yu *et al.*, 2019a). In sharp contrast, GIPC knockdown resulted in Drp1 being distributed diffusely across the cytoplasm with enhanced mitochondrial fusion (Figure 2C, bottom inset panels and Supplemental Figure S1A), suggesting that GIPC is an important determinant of mitochondrial morphology in pancreatic cancer. By gauging the level of mitochondrial connectivity, as reflected by FormFactor analysis and the ratio of cytoplasmic versus perinuclear distribution of Drp1, the combined results suggested that GIPC increases Drp1 transport toward the perinucleus to promote mitochondrial fission (Figure 2, D and E). Consistent with this notion, silencing GIPC expression markedly reduced the level of Drp1 localization at the perinuclear mitochondria compared with control (Figure 2G, colocalization as indicated by yellow in inset panels) and instead facilitated a more tubulated morphology (Figure 2G, inset panels and the Pearson correlation graph).

To further test the role of GIPC in Drp1 localization, we expressed Drp1-WT or Drp1- Δ CT in Drp1-null PDAC cells to find WT present accumulated around the perinucleus just as observed in Drp1+/+ control mouse PDAC cells (Supplemental Figure S2), whereas Drp1- Δ CT localized diffusely across the entire cytoplasm (Figure 3A and graph). Interestingly, the GIPC-Drp1 interaction did not influence the phosphorylation status of the two regulatory sites, Ser616 and Ser637, which are implicated in Drp1 activation and mitochondrial recruitment. Indeed, immunofluorescence staining for phospho-S616 revealed remarkably similar patterns of subcellular distribution as for pan-Drp1 WT or Δ CT (Figure 3B), and biochemical analysis further showed nearly identical levels of p-S616 for WT and the mutant (Figure 3C and below graph), although p-S637 levels were virtually undetectable in both cases (unpublished data). These findings were consistent with the highly fragmented mitochondrial morphology observed in most PDAC cell types due to increased levels of fission-promoting Drp1-S616 phosphorylation while the inhibitory S637 phosphorylation is attenuated (Kashatus *et al.*, 2015; Nagdas *et al.*, 2019).

The above findings indicated that GIPC likely enhances mitochondrial fission via Drp1 transport to the main mitochondrial body and not through phosphorylation. Further consistent with this notion, a strong inverse correlation was observed between increased Drp1-WT expression and reduced fusion, whereas Drp1- Δ CT displayed impaired fission irrespective of increased expression presumably due to their mislocalization (Figure 3D, graphs). But to decisively rule out the possibility that GIPC controls the mitochondrial morphology through Drp1-independent mechanisms, we tested for changes in mitochondrial shape on GIPC overexpression in Drp1+/+ control and Drp1-null PDAC cells (Figure 3E). Results showed significant mitochondrial fission and perinuclear condensation on GIPC overexpression in control cells, whereas a highly tubulated network

of mitochondria persisted in Drp1-null cells irrespective of GIPC expression, thus supporting a critical role for GIPC-dependent Drp1 retrograde transport in promoting mitochondrial fission (Figure 3E, graph).

Because GIPC interacts with MYO6 motor protein to facilitate actin-based retrograde transport of certain cargo proteins, we tested whether Drp1 is also subjected to a similar transport process by using jasplakinolide, a stabilizer of actin filaments. Here, PDAC cells treated with jasplakinolide greatly increased the perinuclear clustering of WT but not Drp1- Δ CT despite enhancing actin polymerization in both cases, thus indicating that the interaction with GIPC is critical for actin-based Drp1 transport (Figure 4A, graph). Conversely, inhibiting actin polymerization with the use of cytochalasin reversed the Drp1-WT localization from highly perinuclear to more diffuse cytoplasmic distribution, as observed for Drp1- Δ CT (Figure 4B, graph). To also consider the possibility of microtubule-based Drp1 trafficking, as is the case for mitochondrial transport, in a parallel experiment PDAC cells were subjected to vinblastine which causes rapid microtubule depolymerization. Here no discernable changes were observed in the overall ratio of cytoplasmic versus perinuclear distribution of either WT or Δ CT despite the decimation of microtubules into free tubulin (Supplemental Figure S3, graph). Together, these findings supported a distinct, actin-specific retrograde transport of Drp1 toward the perinuclear mitochondria mediated by GIPC.

However, we also considered the potential that GIPC promotes mitochondrial fission in part by altering the intrinsic GTPase activity of Drp1. To test this, a series of *in vitro* GTP-binding and hydrolysis assays were performed. First, to assess whether the Drp1 GTP-binding property is controlled by GIPC, we specifically isolated Drp1-WT or Drp1- Δ CT expressed in Drp1-null PDAC cells and measured their ability to bind MANT-GTP, an environment-sensitive GTP analog that enhances fluorescence emission on binding the hydrophobic pocket of GTPases (Kumar *et al.*, 2016). Results here showed negligible difference between WT and Δ CT as evidenced by their potent fluorescence enhancement (Figure 5A and input immunoblot). Second, we employed a GTPase activity assay to ensure that the short C-terminal truncation in Drp1- Δ CT did not cause any structural perturbations that impaired the overall catalytic function. Time-course measurements of GTP hydrolysis revealed that both WT and Δ CT were capable of rapid catalysis in the first 15 min of reaction prior to reaching a plateau (Figure 5B). In addition, the same GTP hydrolysis study was performed in the presence of cardiolipin, a lipid protein previously shown to stimulate Drp1 activity (Macdonald *et al.*, 2014; Stepanyants *et al.*, 2015). Indeed, as shown in Figure 5C, cardiolipin treatment similarly enhanced the GTPase activity of WT and Δ CT over the basal reaction (Figure 5C). Together, these results were consistent with the similar p-S616 levels found in WT and Drp1- Δ CT and thus supported the notion that GIPC enhances mitochondrial fission via Drp1 retrograde trafficking and not by regulating its catalytic function.

Having established a distinct role for GIPC in directed transport of Drp1 that promotes mitochondrial fission, we next tested for major cellular outcomes starting with the production of mitochondria-specific reactive oxygen species (ROS). Measurements using MitoSOX indicated greater mitochondrial superoxide levels in WT than in Drp1- Δ CT expressing mouse PDAC cells, a finding that is consistent with higher mitochondrial fragmentation (Figure 5D). Additionally, we examined for a broad range of cellular processes closely associated with Drp1 including apoptosis, selective autophagy, cell proliferation, and migration. Despite the prominent differences in Drp1 distribution and overall fission, there was surprisingly no

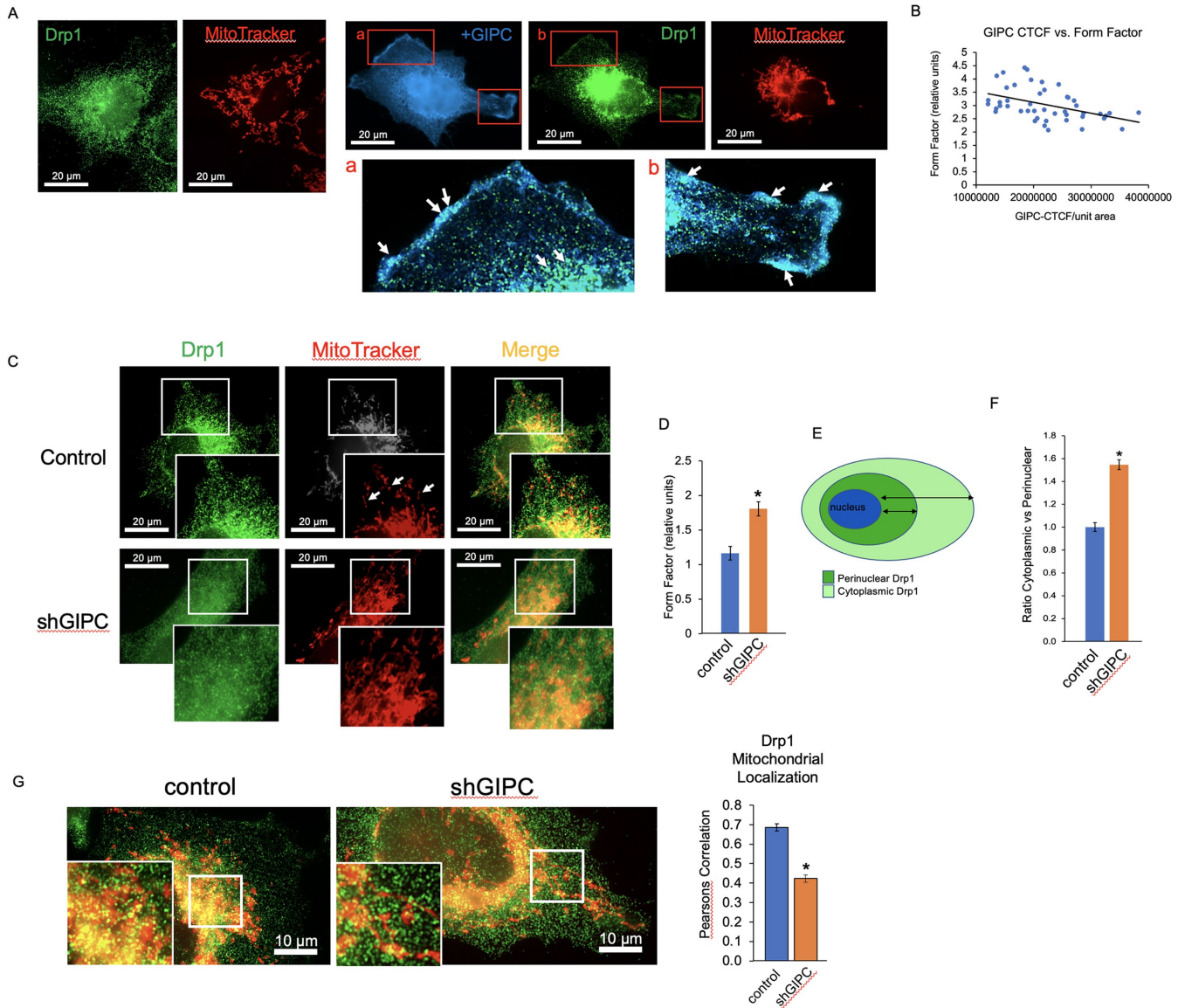


FIGURE 2: GIPC–Drp1 interaction promotes perinuclear clustering and mitochondrial fission. (A) Immunofluorescence reveals more diffuse distribution of endogenous Drp1 (green) and tubulated mitochondria (red MitoTracker) in COS7 cells (left two panels). On GIPC overexpression (blue), it colocalizes with Drp1 (green) at the plasma membrane and perinuclear regions (inset a and b panels and white arrows). MitoTracker staining further demonstrates significant mitochondrial clustering (red). (B) Graph plot shows an inverse relationship between increasing levels of GIPC expression, as assessed by corrected total cell fluorescence (CTCF) and, mitochondrial fusion (Form Factor). Forty cells were quantified for CTCF (fluorescence intensity corrected for cell area) and their form factor. An increase in GIPC causes a decrease in form factor, or more mitochondrial fragmentation. (C) MiaPaca2 (MP2) cells with GIPC1 knockdown (shGIPC) shows more diffuse cytosolic distribution of Drp1 (green) along with increased mitochondrial tubulation (red) compared with control cells that show greater perinuclear accumulation of Drp1 colocalizing with mitochondria (yellow). Also shown are fragmented mitochondria (red) in the cytoplasm of control cells (white arrows). (D) FormFactor was calculated for 25 cells, each with at least two ROIs, from three independent experiments for control and shGIPC1 MiaPaca2 cells. Graph shows an increase in fusion of mitochondria relative to control. $*p < 0.01$. (E) Schematic shows the demarcation method used to quantify the ratio of perinuclear vs. cytoplasmic Drp1 distribution. Drp1 localization was measured from the nucleus to the perinuclear boundary or the cells plasma membrane. (F) Graph represents the relative distribution ratio for control and shGIPC1 MiaPaca2 cells. Twenty cells from three independent experiments were used for quantification. $*p < 0.01$. (G) Immunofluorescence staining of Drp1 and MitoTracker in control and shGIPC1 cells. Inset panels show significant perinuclear clustering of Drp1 and mitochondria (yellow) compared with shGIPC cells that have more tubulated mitochondrial morphology. The Pearson correlation coefficient was calculated for Drp1 on the mitochondria for control and shGIPC1 cells. Thirty representative ROIs were used for Pearson coefficient quantification. $*p < 0.05$.

discernable evidence of change in apoptosis between WT and Δ CT as assessed by PARP and caspase 3 cleavage, two prominent apoptotic markers (unpublished data). In the case of selective autophagy,

immunofluorescence analysis revealed a similar increased presence of LC3 vesicles in Drp1- Δ CT cells at basal state and on chloroquine treatment compared with WT (Figure 6A, below graph). A

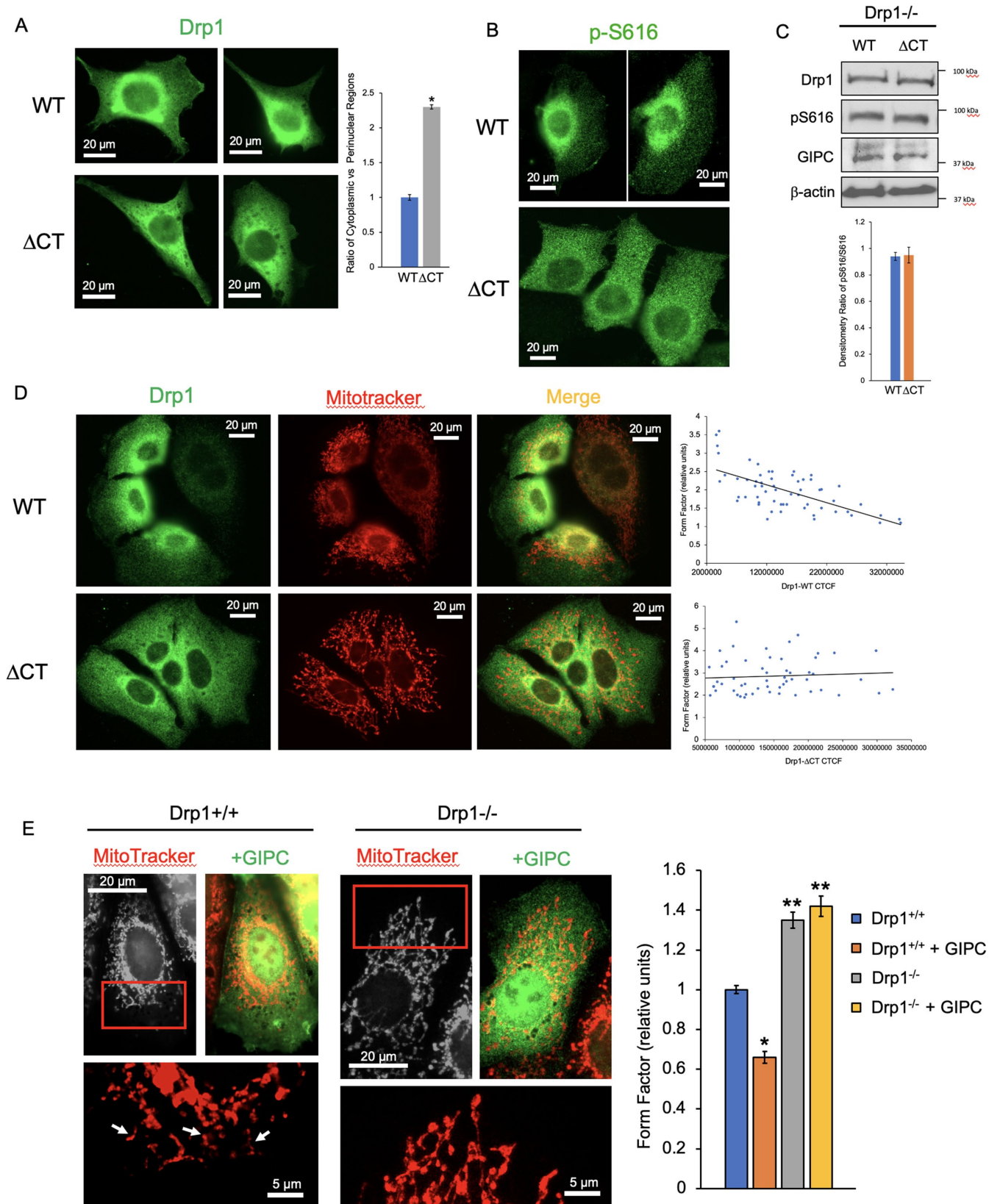


FIGURE 3: Loss of the GIPC–Drp1 interaction causes Drp1 mislocalization and mitochondrial fusion. (A) Immunofluorescence images show the subcellular distribution of Drp1-WT and Drp1- Δ CT transfected in Drp1-null PDAC cells. Graph represents quantification of the cytoplasmic vs. perinuclear accumulation of Drp1. Twenty representative cells total from three independent experiments were used in quantification. * $p < 0.02$. (B) Immunofluorescence images show the subcellular distribution of Drp1-pS616 staining for Drp1-WT and Drp1- Δ CT expressed in Drp1-null PDAC cells. (C) Representative Western blot shows overall Drp1, Drp1-pS616, GIPC, and β -Actin levels in Drp1-null PDAC cells.

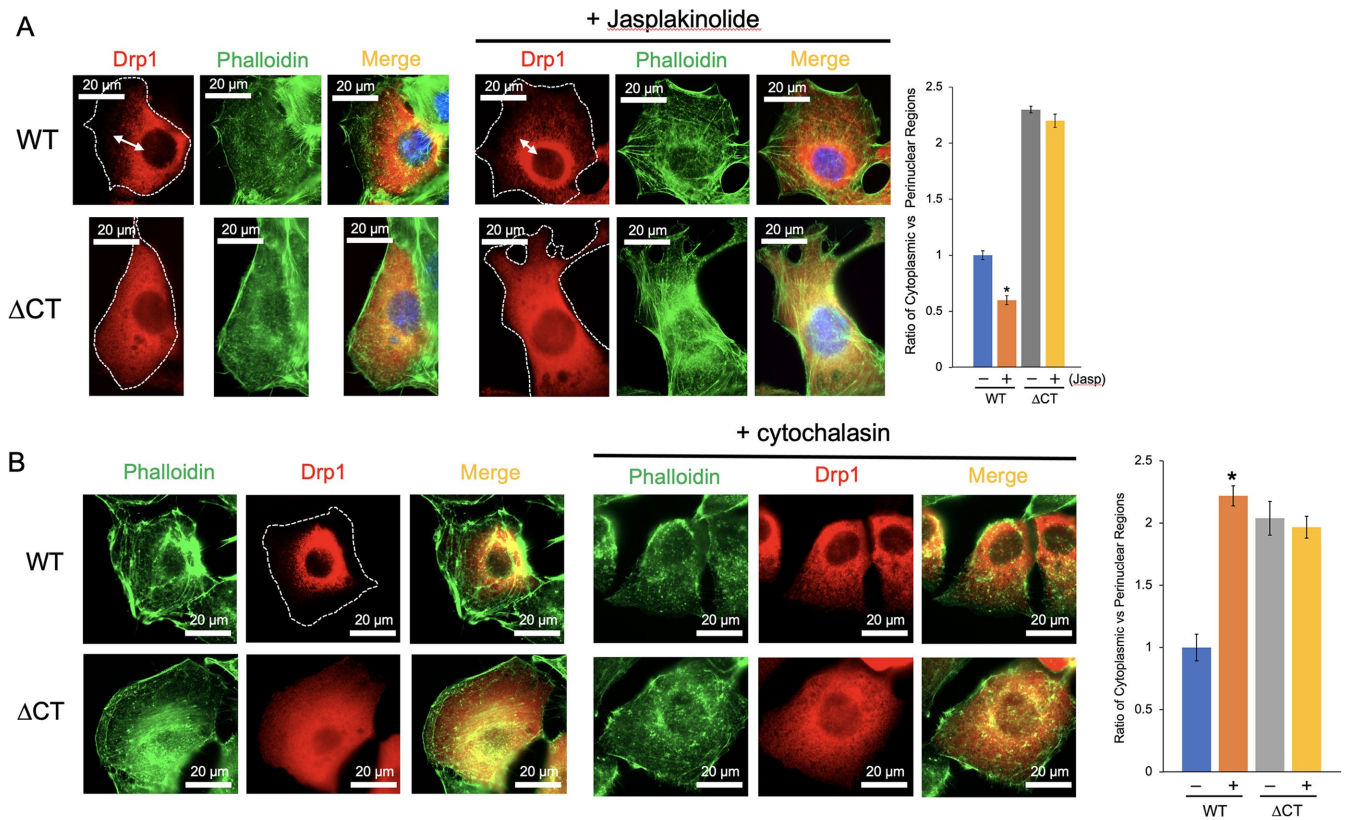


FIGURE 4: GIPC mediates actin-based retrograde Drp1 trafficking. (A) Immunofluorescence images show Drp1-WT vs. Drp1-ΔCT expression in Drp1-null PDAC cells and actin filaments (phalloidin in green) in the presence or absence of jasplakinolide. Graph indicates changes in cytoplasmic vs. perinuclear distribution of Drp1-WT ($*p < 0.05$) but not for Drp1-ΔCT. Ten cells were analyzed in each of three independent experiments for quantification. (B) Immunofluorescence images show Drp1-WT vs. Drp1-ΔCT expression in Drp1-null PDAC cells and actin filaments (phalloidin in green) in the presence or absence of cytochalasin. Graph indicates changes in cytoplasmic vs. perinuclear distribution of Drp1-WT ($*p < 0.01$) but not for Drp1-ΔCT. Ten cells were analyzed in each of three independent experiments for quantification.

subsequent biochemical analysis also showed an increase in LC3 conversion to the lower migrating form, LC3-II, in Drp1-ΔCT-expressing cells especially on chloroquine treatment (Figure 6B). Last, cell proliferation and migration assays both indicated that Drp1-WT more strongly promotes cell growth and migratory behavior in PDAC cells than ΔCT (Figure 6, C and D), a finding consistent with numerous reports linking increased mitochondrial fission with greater invasive motility and tumor cell growth in vitro and in vivo (Rao, 2019).

DISCUSSION

In mammalian systems, mitochondria are actively transported along actin and microtubules in both anterograde and retrograde directions to help maintain their shape, distribution and size (Hollenbeck and Saxton, 2005; Sheng and Cai, 2012; Shen et al., 2018). These directed movements presumably facilitate the local interactions

between mitochondrial surface adaptors and cytosolic Drp1 via Brownian motion, although it is unclear how efficient this process is in accessing the enzyme near the cell periphery and various other distinct cellular compartments. In the present study, we demonstrated that GIPC critically contributes to Drp1 recruitment especially toward the perinuclear mitochondria through an active actin-based retrograde transport system.

Results from our cellular assays are consistent with some of the key roles of Drp1 in promoting proliferation, survival, and migration in cancer. Indeed, as Drp1 is frequently overexpressed in many cancers including PDAC, significant efforts continue to be aimed at understanding how various PTMs influence its turnover, catalytic activity, and the signaling pathways underlying its local recruitment to the mitochondrial surface adaptors. However, regulation of its intracellular transport may be just as vital as we observed that uncoupling the GIPC–Drp1 interaction significantly lowers the rate of

Graph indicates densitometry quantification of three independent experiments. (D) Immunofluorescence images show Drp1 distribution and mitochondrial morphology in PDAC cells overexpressing Drp1-WT or Drp1-ΔCT. CTCF and form factor were calculated and plotted for Drp1-WT and Drp1-ΔCT. As the amount of WT increases more fission is seen, but not for ΔCT. Forty cells total were calculated to generate graph. (E) Immunofluorescence images show PDAC Drp1+/+ and PDAC Drp1-/- cells overexpressing Flag-GIPC (green) while monitoring its effects on mitochondrial morphology with MitoTracker (red). Inset panels and white arrows illustrate the extensive mitochondrial fragmentation observed in Drp1+/+ control but not Drp1-/- cells. FormFactor graph represents the degree of mitochondrial fusion for each group. $*p < 0.05$ and $**p < 0.01$ are relative to Drp1+/+ alone. Quantification was based on 30 cells from three independent experiments.

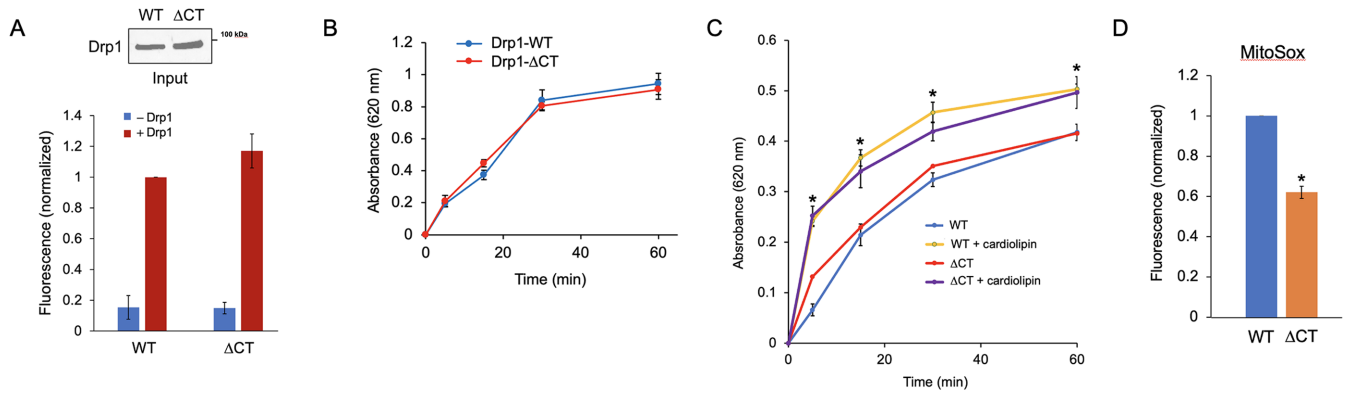


FIGURE 5: GIPC–Drp1 interaction does not influence Drp1 catalytic function. (A) Graph represents MANT-GTP emission in control (blue) or on binding (red) in either Drp1-WT or Drp1-ΔCT isolated from Drp1-null PDAC cells. Error bars represent SE with no statistical significance, between MANT-GTP binding. Inset panel shows a representative immunoblot of equal Drp1 protein loading. (B) Graph represents in vitro GTP hydrolysis of Drp1-WT (blue) and Drp1-ΔCT (red) at indicated time points. Free phosphate was measured by malachite green reagent at an absorbance of 620 nm. Error bars represent SE with no statistical significance in free phosphate levels. (C) Graph represents in vitro GTP hydrolysis assay of Drp1-WT and Drp1-ΔCT in the presence or absence of cardiolipin. Free phosphate was measured by malachite green reagent at an absorbance of 620 nm at different time points. * $p < 0.05$ relative to both WT and Δ-CT under no treatment at each time point. (D) Graph shows mitochondrial superoxide levels as assessed by fluorescence emission on incubation with MitoSOX reagent for WT and ΔCT. * $p < 0.025$

overall fission while reducing the migration and proliferative capacities. These findings therefore represent both physical and functional links between Drp1 and GIPC in regulating mitochondrial functions and further implicate a therapeutic strategy where this interaction could be exploited by peptide-based GIPC inhibitors as an alternative to Drp1-specific inhibitors in certain cancers.

Besides regulating fission, there may be additional functions associated with GIPC-induced translocation to the perinuclear mitochondria. Just as retrograde transport allows for the repair or destruction of damaged mitochondria, Drp1 accumulation in the perinuclear regions may serve a similar purpose of mitochondrial quality control (Vives-Bauza *et al.*, 2010a,b). Along these lines, we observed that selective autophagy was markedly up-regulated on loss of Drp1 transport, although it remains to be determined whether this is a compensatory mechanism to alleviate inefficient mitophagy. Otherwise, GIPC-dependent Drp1 transport could also be involved in regulating Ca^{2+} homeostasis as many have shown that perinuclear mitochondria modulate Ca^{2+} signals by uptake, buffering, and releasing Ca^{2+} at key locations near Ca^{2+} release or influx channels (Park *et al.*, 2001; Frieden *et al.*, 2004).

Our data suggest that GIPC promotes mitochondrial fission primarily by coordinating Drp1 trafficking and not its intrinsic GTPase activity as both WT and Drp1-ΔCT displayed efficient MANT-GTP-binding properties. Similarly, the nearly identical rate at which the two isolated proteins hydrolyzed GTP in solution at basal and cardiolipin-induced states further supports the notion that deleting the C-terminal PDZ motif does not profoundly impair its enzymatic function. However, whether Drp1-ΔCT can form oligomeric structures around the mitochondrial assembly sites as efficiently as WT remains to be more fully investigated. Studies have shown that Drp1 requires receptor-mediated oligomerization at the scission sites involving MiD49 and MiD51 as well as external assistance from actin filaments along the ER-mitochondria contact sites to facilitate mitochondrial outer membrane constriction (Macdonald *et al.*, 2014; Stepanyants *et al.*, 2015; Cho *et al.*, 2017). While beyond the scope of the present study, it will be important to determine how the GIPC–Drp1 interaction is influenced by the fission machinery. Nevertheless, the fact that the overall level of S616-phosphorylated

Drp1 was not altered indicates that its interaction with GIPC and directed transport does not interfere with its intrinsic GTPase functions. In the case of the Ser637 phosphorylation, it is not entirely clear why we failed to detect its signal in either WT or Drp1-ΔCT, although it is plausible that the Drp1-null PDAC cells do not have high PKA activity or, conversely, have high phosphatase activity toward this site. But it is unlikely that this site contributes to Drp1 retrograde transport for two reasons. First, contrary to expectations, a recent study showed that the phosphorylation status of Ser637 does not determine Drp1 recruitment to the mitochondria as S637-phosphorylated Drp1 resides in both the cytosol and the mitochondrial surface and proves fully capable of interacting with mitochondrial adaptors Mff and MiD49/51 (Yu *et al.*, 2019b). Second, our overall findings are consistent with the phosphorylation characteristics that reflect constitutively high Drp1 activity and excessive mitochondrial fragmentation as observed in most PDAC cells types.

There are numerous additional questions arising from our present study. First and foremost, the presence of a retrograde transport system suggests that there is also an anterograde transport to shuttle Drp1 between the perinuclear mitochondria and the cell periphery. Fully defining these mechanisms will be crucial in understanding how directed Drp1 transport fits into the already complex multistep process of mitochondrial fission, and their defects may be related to the pathogenesis of numerous Drp1-related neurologic, metabolic, and malignant disorders. Second, given that Drp1 also promotes division of peroxisomes (Kamerkar *et al.*, 2018), it will be important to examine how GIPC influences fatty acid oxidation, lipid synthesis, and ROS generation. Third, the fact that PDZ-binding motifs often comprise a serine or threonine, it is possible that the threonine residue present in the THLW motif serves as a phosphoregulatory site for the GIPC–Drp1 interaction. Indeed, previous studies have shown that serine/threonine phosphorylation within the PDZ-binding motif can either promote or inhibit GIPC interaction depending on the substrate (Lee and Zheng, 2010; Toto *et al.*, 2017). Based on our newly discovered GIPC–Drp1 interaction, it will be important to establish whether this association is constitutive or is actively governed by upstream kinases, phosphatases, and cellular contexts including growth factor signaling, metabolic changes, and stress.

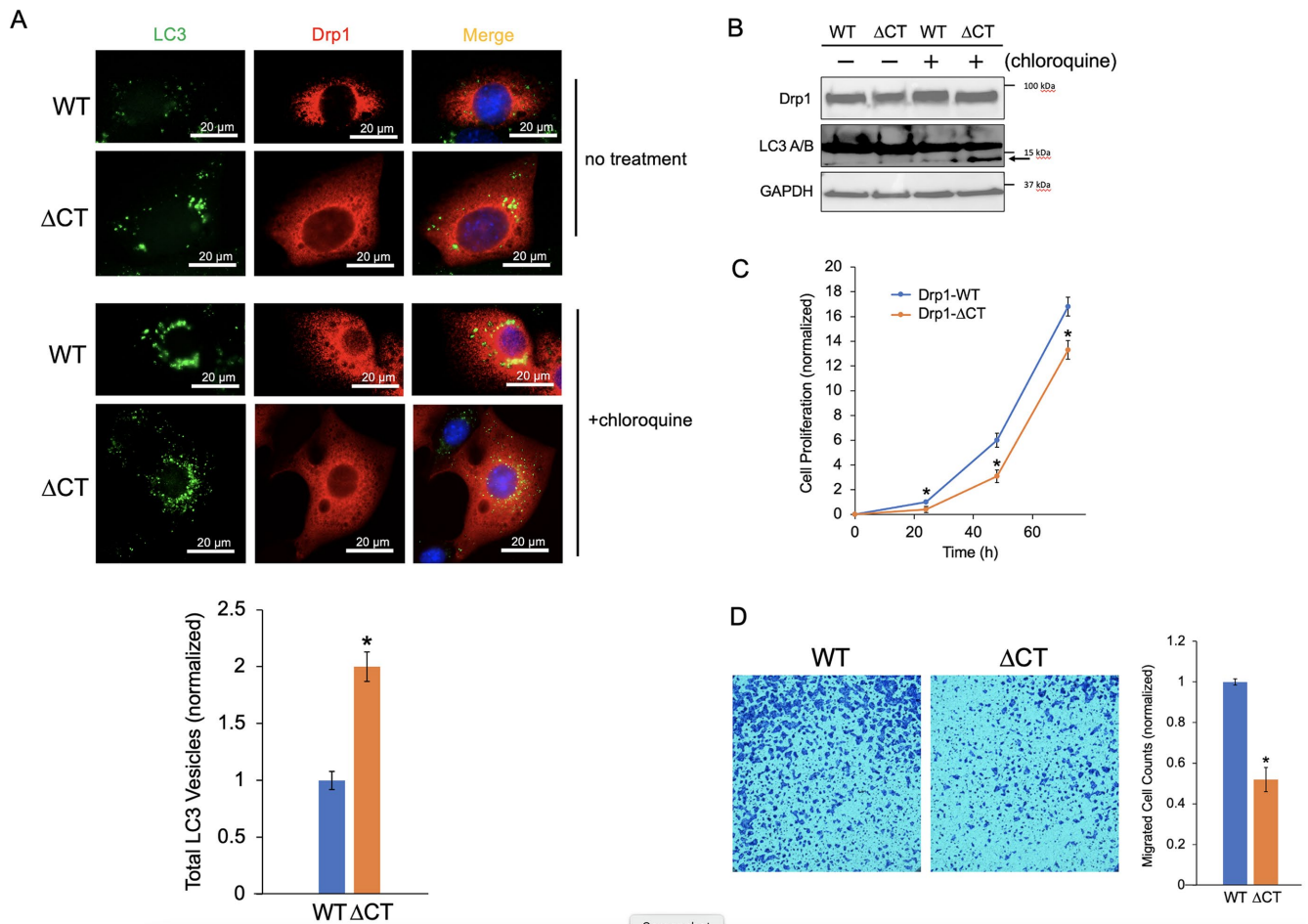


FIGURE 6: GIPC–Drp1 interaction enhances cell growth and migration. (A) Immunofluorescence images show punctate LC3 vesicles indicative of selective autophagy in WT or ΔCT expressing Drp1-null PDAC cells in the presence or absence of chloroquine treatment. Graph quantifies the total LC3 punctate vesicles per cell. Thirty cells were counted in three independent experiments. * $p < 0.01$ relative to WT. (B) Western blot compares the level of selective autophagy, as assessed by LC3 cleavage in the presence or absence of chloroquine. More LC3 accumulation is seen in ΔCT (indicated by the black arrow). (C) Graph represents cell proliferation of WT and ΔCT expressing Drp1-null PDAC cells over 72 h as assessed by crystal violet absorbance readings normalized to Drp1-WT. * $P < 0.05$ over WT. (D) Representative images of transwell migration and graph comparing the total cell migration between WT and ΔCT expressing Drp1-null PDAC cells. * $p < 0.035$ over WT.

In summary, here we present an important new facet of mitochondrial dynamics as results show that GIPC, a highly versatile endocytic trafficking adaptor protein, is a key regulator of mitochondrial fission. We find that GIPC directly interacts with a previously undefined PDZ binding motif of Drp1 to coordinate its retrograde transport toward the perinuclear mitochondria. This directed movement marks the first evidence of how Drp1 requires active intracellular transport in addition to the adaptor machinery for efficient mitochondrial recruitment and fission activities. As the expression of GIPC and Drp1 is closely linked to many malignant, neurologic, and metabolic disorders, these findings reveal unique pathophysiologic implications and therapeutic perspectives.

MATERIALS AND METHODS

[Request a protocol](#) through *Bio-protocol*.

Antibodies

Antibodies used in this study include Drp1, pDrp1 S616, α -tubulin, LC3 A/B, GAPDH, and MFN2 (all from Cell Signaling); HA, Flag, and β -Actin (all from Sigma); and GIPC (from Santa Cruz) (Table 1).

Plasmids

Drp1-WT and Drp1-ΔCT were generated through IDT custom gene synthesis. Briefly, full-length human Drp1 sequence was generated through synthetic gene construction while Drp1-ΔCT lacked the 3'-end sequence corresponding to THLW. These constructs were then subcloned into pcDNA3.1 for further use.

Cell culture and transfection

COS-7 and MiaPaCa2 cells were purchased from ATCC. Control mouse and Drp1-null PDAC cells were generous gifts from Kashatus. Cells were cultured in DMEM (Gibco) supplemented with 10% fetal bovine serum (FBS) (Gibco). MP2 shGIPC knockdown stables were generated first by small hairpin RNA vector transfection, selected in puromycin (5–10 μ g/ml), then colonies were isolated and biochemically validated for GIPC1 knockdown. Transfection was performed using Lipofectamine 2000 (Invitrogen). Standard immunoprecipitation and immunoblotting were prepared in lysis buffer (20 mM HEPES [pH 7.4], 150 mM NaCl, 2 mM EDTA, 10 mM NaF, 10% [wt/vol] glycerol, 1% NP-40) supplemented with protease inhibitors (Sigma) and phosphatase inhibitors (Sigma).

Reagent or resource	Source	Identifier
Antibodies		
GIPC (B-12)	Santa Cruz Biotechnology	sc-271822, RRID:AB_10707672
Monoclonal ANTI-FLAG M2 antibody	Sigma-Aldrich	Cat# F1804, RRID:AB_262044
GIPC (H-55)	Santa Cruz Biotechnology	Cat# sc-25556, RRID:AB_2109830
Anti- β -actin	Sigma-Aldrich	Cat# A1978, RRID:AB_476692
DRP1 (D6C7) rabbit mAb antibody	Cell Signaling Technology	Cat# 8570, RRID:AB_10950498
DRP1, phospho (Ser616) polyclonal antibody	Cell Signaling Technology	Cat# 3455, RRID:AB_2085352
LC3A/B (D3U4C) XP antibody	Cell Signaling Technology	Cat# 13173, RRID:AB_2728823
GAPDH (D16H11) XP rabbit mAb antibody	Cell Signaling Technology	Cat# 5174, RRID:AB_10622025
Anti-HA high affinity; rat monoclonal antibody (clone 3F10)	Roche	Cat# 11867423001, RRID:AB_390918
Alpha tubulin (YOL1/34) antibody	Santa Cruz Biotechnology	Cat# sc-53030, RRID:AB_2272440
Mouse IgG normal antibody	Millipore	Cat# NI03-100UG, RRID:AB_10683482
Mfn-2 (D1E9) antibody	Cell Signaling Technology	Cat# 11925, RRID:AB_2750893
DRP1, phospho (637) antibody	Cell Signaling Technology	Cat# 4867
Bacterial and virus strains		
Biological samples		
Chemicals, peptides, and recombinant proteins		
Lipofectamine 2000 transfection reagent	Thermo Fisher Scientific	Cat# 11668027
Vinblastine sulfate salt	Millipore	Cat# V1377-5MG
Cytochalasin D	Thermo Fisher Scientific	Cat# PHZ1063
Cardiolipin	Avanti Polar Lipids	Cat# 840012
Jasplakinolide	Santa Cruz Biotechnology	Cat# sc-202191
MANT-GTP (2'-(or-3')-O-(N-methylanthraniloyl) guanosine 5'-triphosphate, trisodium salt)	Thermo Fisher Scientific	Cat# M12415
Guanosine 5'-triphosphate	Cytiva	Cat# GE27-2076-01
MitoSOX red mitochondrial superoxide indicator	Thermo Fisher Scientific	Cat# M36008
Chloroquine diphosphate salt	Millipore	Cat# C6628
Mitotracker Red CMXRos	Thermo Fisher Scientific	Cat# M7512
Critical commercial assays		
QuantiChrom GTPase assay kit	BioAssay Systems	Cat# DATG-200
Deposited data		
Experimental models: cell lines		
Monkey kidney fibroblast cells (COS-7)	ATCC	Cat# CRL-1651, RRID:CVCL_0224
Human pancreatic carcinoma (MIA PaCa-2 or MP2)	ATCC	Cat# CRM-CRL-1420, RRID:CVCL_0428
Mouse primary PDAC	Laboratory of David Kashatus (University of Virginia)	N/A
Experimental models: organisms/strains		
Oligonucleotides		
Recombinant DNA		
Control shRNA plasmid	Santa Cruz Biotechnology	
Plasmid: HA-DRP1 WT	This paper	
Plasmid: HA- DRP1 Δ CT	This paper	
Plasmid: Flag-GIPC1	This paper	
Plasmid: GIPC1 MISSION shRNA	Sigma-Aldrich	TRCN0000036771
Plasmid: GIPC1 MISSION shRNA	Sigma-Aldrich	TRCN0000289265

TABLE 1: Reagents and resources.

(Continues)

Reagent or resource	Source	Identifier
Plasmid: ER-mRFP	Addgene	
Plasmid: peroxisome-Scarlett	Addgene	
Software and algorithms		
ImageJ		
Adobe Photoshop		
Excel		
ANOVA		

TABLE 1: Reagents and resources. Continued

Immunoprecipitation assays

Cells were washed with phosphate-buffered saline (PBS), lysed on ice with lysis buffer for 20 min (20 mM HEPES [pH 7.4], 150 mM NaCl, 2 mM EDTA, 10 mM NaF, 10% [wt/vol] glycerol, and 1% NP-40) prior to centrifugation at 13,000 RPM for 15 min. Supernatants were incubated with appropriate antibodies and agarose G or Protein A agarose for 4–6 h at 4°C. Immunoprecipitants were then washed three times then stored in 2× sample buffer prior to Western blot analyses.

Immunofluorescence studies, form factor, and Pearson coefficient calculations

Cells grown on coverslips were fixed with 4% paraformaldehyde, permeabilized in 0.1% Triton X-100 in PBS for 3 min, then blocked with 5% bovine serum albumin (BSA)/0.05% Triton X-100 PBS for 20 min. All primary antibodies were incubated in 5% BSA/0.05% Triton X-100 PBS for 1 h at RT, and fluorescently conjugated secondary antibodies were incubated at room temperature for 30 min. Mitochondrial morphology assessment was based on calculating form factor, an average of isolated mitochondrial particles in a region of interest (ROI). Raw images obtained from immunofluorescence microscope were binarized and quantified based on ImageJ using Mito Morphology Macro (Dagda *et al.*, 2009). Form factor for each mitochondrion was calculated and averaged in Excel for each cell. For the Pearson coefficient calculations, all quantifications were performed on FIJI using the JACoP plugin. Small ROIs were taken per cell for colocalization measurement.

DRP1-GTPase activation assay

Cells were immunoprecipitated in GTPase lysis buffer (20 mM HEPES [pH 7.4], 150 mM NaCl, 5 mM NaF, and 1% NP-40) with appropriate antibodies, then washed and resuspended with GTPase lysis buffer. The immunocomplexes were incubated with MANT-GTP at 2.5 μM final concentration and mixed for 1 min prior to transferring each immunocomplex into quadruplicates in a 96-well fluorescence plate. Additional mixing was performed in three 30-s bursts in the fluorescence 96-well plate reader (CLARIOstar) at 25°C prior to fluorescence measurements at 360 nm_{ex} and 440 nm_{em} using bottom fluorescence area scan (5 × 5). Control fluorescence emission was subtracted from the experimental readings prior to relative normalization of data to fluorescence emission of Drp1 WT.

DRP1- GTPase malachite free phosphate assay with cardiolipin stimulation

ATPase/ GTPase Assay Kit (QuantiChrom). Cells were immunoprecipitated in GTPase lysis buffer (20 mM HEPES [pH 7.4], 150 mM NaCl, and 5 mM NaF, 1% NP-40) with appropriate antibodies, then washed and resuspended with GTPase lysis buffer. After the final

wash, the immunoprecipitants were resuspended in assay buffer (QuantiChrom) and incubated with 1 mM GTP for the desired time at RT. For cardiolipin stimulation, 150 μM of total lipid was incubated at 37°C with immunoprecipitants for 30 min before the addition of GTP. After incubation with GTP, malachite reagent was added and allowed 30 min to react with free phosphate. The supernatant was then transferred to a 96-well absorbance plate in triplicates. Bottom area scan was used to measure optical density at 620 nm. Concentrations were then determined from absorbance values using the calibration curve of known free phosphate concentrations.

Mitochondrial ROS assay

Mitochondrial superoxide production was measured using the MitoSOX Red mitochondrial superoxide indicator fluorescent probe (Invitrogen). Cells grown and transfected in 96-well plates were washed twice with PBS and subsequently incubated for 10 min with Mitosox Red (5 μM) at 37°C. After the incubation, fluorescence was measured with a microplate reader set to 510-nm excitation 580-nm emission wavelengths.

Crystal violet growth assay

PDAC cells with ectopically transfected Drp1 WT and Drp1-ΔCT were plated in 12-well plates at quadruplicates. Cells were fixed with 4% paraformaldehyde for 15 min at different time points starting at 24 h posttransfection. Following fixation, cells were washed with water once and stained with 0.1% crystal violet for 30 min. Cells were washed with water repeatedly and air-dried for 30 min. Cells were destained using crystal violet destaining solution (10% acetic acid, 50% methanol, and 40% water) for 15 min, and the optical density was read at 590 nm in a microplate reader.

Jasplakinolide, cytochalasin D, and vinblastine-dependent Drp1 distribution measurements

Drp1^{-/-} PDAC cells expressing Drp1-WT or Drp1-ΔCT were subjected to jasplakinolide, cytochalasin-D, or vinblastine treatment to measure Drp1 cytoplasmic distribution. Cells were treated with 50 nM jasplakinolide for 1 h prior to fixation with 4% paraformaldehyde. The fixed cells were stained for Drp1 and phalloidin for immunofluorescence analysis. Cells were treated with 1.5 μM vinblastine for 1 h prior to fixation with 4% paraformaldehyde. The fixed cells were then stained for Drp1 and α-tubulin for immunofluorescence analysis. Cells were treated with 0.3 μM of cytochalasin D for 30 min prior to fixation with 4% paraformaldehyde then stained for Drp1 and phalloidin. All immunofluorescence staining followed the methods for staining as seen in this paper. Images were then analyzed on ImageJ/FIJI application to measure DRP1 cytoplasmic distribution. Distribution was measured by the length from the

nucleus to edge of Drp1 perinuclear boundary over the distance from the nucleus to the plasma membrane. This value gives a ratio of the perinuclear and cytoplasmic portions of Drp1 in the cell.

Cell migration assay

PDAC Drp1^{-/-} cells expressing Drp1 WT or Drp1-ΔCT were plated in a transmembrane migration well in DMEM w/o 10% FBS; the bottom well was filled with DMEM w/10% FBS. Cells were plated and placed in incubator for 18 h at 37°C, prior to fixing and staining. Images were taken of the membrane, and ImageJ/FIJI application was used to analyze the amount of cells that migrated through the membrane.

Western blotting

Cell lysates were separated by SDS-PAGE and electrophoretically transferred onto the polyvinylidene difluoride membranes (Bio-Rad). Transferred membranes were blocked with 5% skim milk in Tris-buffered saline (TBS) with 0.1% Tween-20 and then incubated with primary antibodies at 4°C overnight. The following day, membranes were washed three times in TBS buffer with 0.1% Tween-20 and incubated with the secondary antibody for 45 min at room temperature. Membranes were washed five times in TBS buffer with 0.1% Tween-20 each 5 min then imaged by ChemiDoc Imaging system (Bio-Rad).

ACKNOWLEDGMENTS

We thank the University of Arizona Cancer Center for their assistance. This work was supported in part by the internal funding provided by the University of Arizona Cancer Center and College of Medicine.

REFERENCES

Ahmed T, Myhre K, Lee NY (2021). Strength and duration of GIPC-dependent signaling networks as determinants in cancer. *Neoplasia* 23, 181–188.

Archer SL (2013). Mitochondrial dynamics—mitochondrial fission and fusion in human diseases. *N Engl J Med* 369, 2236–2251.

Breitzig MT, Alleyn MD, Lockey RF, Kolliputi N (2018). A mitochondrial delicacy: dynamin-related protein 1 and mitochondrial dynamics. *Am J Physiol Cell Physiol* 315, C80–C90.

Chang CR, Blackstone C (2007a). Cyclic AMP-dependent protein kinase phosphorylation of Drp1 regulates its GTPase activity and mitochondrial morphology. *J Biol Chem* 282, 21583–21587.

Chang CR, Blackstone C (2007b). Drp1 phosphorylation and mitochondrial regulation. *EMBO Rep* 8, 1088–1089; author reply 1089–1090.

Chang CR, Blackstone C (2010). Dynamic regulation of mitochondrial fission through modification of the dynamin-related protein Drp1. *Ann NY Acad Sci* 1201, 34–39.

Chen H, Detmer SA, Ewald AJ, Griffin EE, Fraser SE, Chan DC (2003). Mitofusins Mfn1 and Mfn2 coordinately regulate mitochondrial fusion and are essential for embryonic development. *J Cell Biol* 160, 189–200.

Chittenden TW, Pak J, Rubio R, Cheng H, Holton K, Prendergast N, Glinski V, Cai Y, Culhane A, Bentink S, et al. (2010). Therapeutic implications of GIPC1 silencing in cancer. *PLoS One* 5, e15581.

Cho B, Cho HM, Jo Y, Kim HD, Song M, Moon C, Kim H, Kim K, Sesaki H, Rhyu IJ, et al. (2017). Constriction of the mitochondrial inner compartment is a priming event for mitochondrial division. *Nat Commun* 8, 15754.

Cipolat S, Martins de Brito O, Dal Zilio B, Scorrano L (2004). OPA1 requires mitofusin 1 to promote mitochondrial fusion. *Proc Natl Acad Sci USA* 101, 15927–15932.

Dagda RK, Cherra SJ, 3rd, Kulich SM, Tandon A, Park D, Chu CT (2009). Loss of PINK1 function promotes mitophagy through effects on oxidative stress and mitochondrial fission. *J Biol Chem* 284, 13843–13855.

Frank S, Gaume B, Bergmann-Leitner ES, Leitner WW, Robert EG, Catez F, Smith CL, Youle RJ (2001). The role of dynamin-related protein 1, a mediator of mitochondrial fission, in apoptosis. *Dev Cell* 1, 515–525.

Frieden M, James D, Castelbou C, Danckaert A, Martinou JC, Demaurex N (2004). Ca²⁺ homeostasis during mitochondrial fragmentation and perinuclear clustering induced by hFis1. *J Biol Chem* 279, 22704–22714.

Hales KG, Fuller MT (1997). Developmentally regulated mitochondrial fusion mediated by a conserved, novel, predicted GTPase. *Cell* 90, 121–129.

Hollenbeck PJ, Saxton WM (2005). The axonal transport of mitochondria. *J Cell Sci* 118, 5411–5419.

Ji WK, Chakrabarti R, Fan X, Schoenfeld L, Strack S, Higgs HN (2017). Receptor-mediated Drp1 oligomerization on endoplasmic reticulum. *J Cell Biol* 216, 4123–4139.

Kamerkar SC, Kraus F, Sharpe AJ, Pucadyil TJ, Ryan MT (2018). Dynamin-related protein 1 has membrane constricting and severing abilities sufficient for mitochondrial and peroxisomal fission. *Nat Commun* 9, 5239.

Kashatus JA, Nascimento A, Myers LJ, Sher A, Byrne FL, Hoehn KL, Counter CM, Kashatus DF (2015). Erk2 phosphorylation of Drp1 promotes mitochondrial fission and MAPK-driven tumor growth. *Mol Cell* 57, 537–551.

Katoh M (2013). Functional proteomics, human genetics and cancer biology of GIPC family members. *Exp Mol Med* 45, e26.

Kraus F, Ryan MT (2017). The constriction and scission machineries involved in mitochondrial fission. *J Cell Sci* 130, 2953–2960.

Kumar S, Pan CC, Shah N, Wheeler SE, Hoyt KR, Hempel N, Myhre K, Lee NY (2016). Activation of mitofusin2 by Smad2-RIN1 complex during mitochondrial fusion. *Mol Cell* 62, 520–531.

La Torre A, Hoshino A, Cavanaugh C, Ware CB, Reh TA. (2015). The GIPC1-Akt1 pathway is required for the specification of the eye field in mouse embryonic stem cells. *Stem Cells* 33, 2674–2685.

Lackner LL (2014). Shaping the dynamic mitochondrial network. *BMC Biol* 12, 35.

Lee NY, Golzio C, Gatza CE, Sharma A, Katsanis N, Blobel GC (2012). Endoglin regulates PI3-kinase/Akt trafficking and signaling to alter endothelial capillary stability during angiogenesis. *Mol Biol Cell* 23, 2412–2423.

Lee JD, Hempel N, Lee NY, Blobel GC (2010). The type III TGF-beta receptor suppresses breast cancer progression through GIPC-mediated inhibition of TGF-beta signaling. *Carcinogenesis* 31, 175–183.

Lee HJ, Zheng JJ (2010). PDZ domains and their binding partners: structure, specificity, and modification. *Cell Commun Signal* 8, 8.

Loson OC, Song Z, Chen H, Chan DC (2013). Fis1, Mff, MiD49, and MiD51 mediate Drp1 recruitment in mitochondrial fission. *Mol Biol Cell* 24, 659–667.

Macdonald PJ, Stepanyants N, Mehrotra N, Mears JA, Qi X, Sesaki H, Ramachandran R (2014). A dimeric equilibrium intermediate nucleates Drp1 reassembly on mitochondrial membranes for fission. *Mol Biol Cell* 25, 1905–1915.

Muders MH, Vohra PK, Dutta SK, Wang E, Ikeda Y, Wang L, Udugamasooriya DG, Memic A, Rupasinghe CN, Baretton GB, et al. (2009). Targeting GIPC/synectin in pancreatic cancer inhibits tumor growth. *Clin Cancer Res* 15, 4095–4103.

Naccache SN, Hasson T, Horowitz A (2006). Binding of internalized receptors to the PDZ domain of GIPC/synectin recruits myosin VI to endocytic vesicles. *Proc Natl Acad Sci USA* 103, 12735–12740.

Nagdas S, Kashatus JA, Nascimento A, Hussain SS, Trainor RE, Pollock SR, Adair SJ, Michaels AD, Sesaki H, Stelov EB, et al. (2019). Drp1 promotes KRas-driven metabolic changes to drive pancreatic tumor growth. *Cell Rep* 28, 1845–1859.e1845.

Otera H, Wang C, Cleland MM, Setoguchi K, Yokota S, Youle RJ, Mihara K (2010). Mff is an essential factor for mitochondrial recruitment of Drp1 during mitochondrial fission in mammalian cells. *J Cell Biol* 191, 1141–1158.

Pal K, Pletnev AA, Dutta SK, Wang E, Zhao R, Baral A, Yadav VK, Aggarwal S, Krishnaswamy S, Alkharfy KM, et al. (2014). Inhibition of endoglin-GIPC interaction inhibits pancreatic cancer cell growth. *Mol Cancer Ther* 13, 2264–2275.

Palmer CS, Elgass KD, Parton RG, Osellame LD, Stojanovski D, Ryan MT (2013). Adaptor proteins MiD49 and MiD51 can act independently of Mff and Fis1 in Drp1 recruitment and are specific for mitochondrial fission. *J Biol Chem* 288, 27584–27593.

Park MK, Ashby MC, Erdemli G, Petersen OH, Tepikin AV (2001). Perinuclear, perigranular and sub-plasmalemmal mitochondria have distinct functions in the regulation of cellular calcium transport. *EMBO J* 20, 1863–1874.

Ranieri M, Brajkovic S, Riboldi G, Ronchi D, Rizzo F, Bresolin N, Corti S, Comi GP (2013). Mitochondrial fusion proteins and human diseases. *Neurol Res Int* 2013, 293893.

Rao VA (2019). Targeting mitochondrial fission to trigger cancer cell death. *Cancer Res* 79, 6074–6075.

- Samangouei P, Crespo-Avilan GE, Cabrera-Fuentes H, Hernandez-Resendiz S, Ismail NI, Katwadi KB, Boisvert WA, Hausenloy DJ (2018). MiD49 and MiD51: New mediators of mitochondrial fission and novel targets for cardioprotection. *Cond Med* 1, 239–246.
- Santel A, Frank S (2008). Shaping mitochondria: The complex posttranslational regulation of the mitochondrial fission protein DRP1. *IUBMB Life* 60, 448–455.
- Serasinghe MN, Wieder SY, Renault TT, Elkholi R, Ascioia JJ, Yao JL, Jabado O, Hoehn K, Kageyama Y, Sesaki H, Chipuk JE (2015). Mitochondrial division is requisite to RAS-induced transformation and targeted by oncogenic MAPK pathway inhibitors. *Mol Cell* 57, 521–536.
- Shen J, Zhang JH, Xiao H, Wu JM, He KM, Lv ZZ, Li ZJ, Xu M, Zhang YY (2018). Mitochondria are transported along microtubules in membrane nanotubes to rescue distressed cardiomyocytes from apoptosis. *Cell Death Dis* 9, 81.
- Sheng ZH, Cai Q (2012). Mitochondrial transport in neurons: impact on synaptic homeostasis and neurodegeneration. *Nat Rev Neurosci* 13, 77–93.
- Stepanyants N, Macdonald PJ, Francy CA, Mears JA, Qi X, Ramachandran R (2015). Cardiolipin's propensity for phase transition and its reorganization by dynamin-related protein 1 form a basis for mitochondrial membrane fission. *Mol Biol Cell* 26, 3104–3116.
- Toto A, Mattei A, Jemth P, Gianni S (2017). Understanding the role of phosphorylation in the binding mechanism of a PDZ domain. *Protein Eng Des Sel* 30, 1–5.
- Valdembri D, Caswell PT, Anderson KI, Schwarz JP, Konig I, Astanina E, Caccavari F, Norman JC, Humphries MJ, Bussolino F, Serini G (2009). Neuropilin-1/GIPC1 signaling regulates alpha5beta1 integrin traffic and function in endothelial cells. *PLoS Biol* 7, e25.
- Vives-Bauza C, de Vries RL, Tocilescu M, Przedborski S (2010a). PINK1/Par-kin direct mitochondria to autophagy. *Autophagy* 6, 315–316.
- Vives-Bauza C, Zhou C, Huang Y, Cui M, de Vries RL, Kim J, May J, Tocilescu MA, Liu W, Ko HS, *et al.* (2010b). PINK1-dependent recruitment of Par-kin to mitochondria in mitophagy. *Proc Natl Acad Sci USA* 107, 378–383.
- Wells AL, Lin AW, Chen LQ, Safer D, Cain SM, Hasson T, Carragher BO, Milligan RA, Sweeney HL (1999). Myosin VI is an actin-based motor that moves backwards. *Nature* 401, 505–508.
- Yu M, Nguyen ND, Huang Y, Lin D, Fujimoto TN, Molkentine JM, Deorukhkar A, Kang Y, San Lucas FA, Fernandes CJ, *et al.* (2019a). Mitochondrial fusion exploits a therapeutic vulnerability of pancreatic cancer. *JCI Insight* 5. 10.1172/jci.insight.126915.
- Yu R, Liu T, Ning C, Tan F, Jin SB, Lendahl U, Zhao J, Nister M (2019b). The phosphorylation status of Ser-637 in dynamin-related protein 1 (Drp1) does not determine Drp1 recruitment to mitochondria. *J Biol Chem* 294, 17262–17277.